Journal of Crystal Growth 318 (2011) 59–65

Contents lists available at ScienceDirect

Journal of Crystal Growth

journal homepage: www.elsevier.com/locate/jcrysgro

The effect of structure on tensile properties of directionally solidified Zn-based alloys

A.E. Ares [a,b,*], C.E. Schvezov [a,b]

[a] Member of CIC of the National Research Council of Argentina (CONICET), 1552 Félix de Azara Street, 3300 Posadas-Misiones, Argentina
[b] University of Misiones, 1552 Félix de Azara Street, 3300 Posadas-Misiones, Argentina

ARTICLE INFO

Available online 2 December 2010

Keywords:
A1. Columnar-to-equiaxed grain transition
A1. Directional solidification
A1. Dendrites
A1. Mechanical properties
A2. Growth from melt
B1. Alloys

ABSTRACT

The main objective of this study was to measure thermal (cooling rates, temperature gradients and velocities of the liquidus and solidus isotherms), structural (grain size and primary and secondary dendritic arm spacings) and tensile parameters (maximum tensile strength (MTS), yield strength (YS) and ultimate tensile strength (UTS)) in zinc–aluminum (ZA) hypoeutectic (Zn–3 wt%Al) and hypereutectic (Zn–10 wt%Al, Zn–15 wt%Al, Zn–20 wt%Al, Zn–30 wt%Al, Zn–37 wt%Al and Zn–50 wt%Al) alloys directionally solidified, which present columnar, equiaxed and columnar-to-equiaxed transition (CET) structures. The different types of structures were analyzed with optical and Scanning Electron Microscopy (SEM). Correlations between temperature gradient, cooling rate, local solidification time, grain size and dendritic spacings and tensile tests parameters are presented and discussed. The results show the influence of concentration, microstructural arrangement and thermal conditions on the mechanical properties during the solidification process.

1. Introduction

Molten and solid zinc-rich alloys with high aluminum content and small amounts of alloying elements have been a field of interest in recent years [1]. Aluminum increases the fluidity of the alloy and improves its mechanical properties [1,2]. The mechanical properties of an alloy depend on the solidification microstructural arrangement (primary and secondary spacings and grain size) [1–3]. In order to use metals and alloys in particular applications, it is necessary to know their tensile strength (TS), particularly the maximum tensile strength (MTS) and yield strength (YS) [4–6]. Also, it is very important to know the relationship between the tensile, structure and thermal parameters.

The Hall–Petch equation is well known and predicts that as the grain diameter decreases the yield strength increases [7,8]. However, this equation is true for equiaxed growth and absence of defects in the sample, such as the amount of microporosity or the volume percentage of second phases [9].

We have previously carried out experiments in which the conditions of the columnar-to-equiaxed transition (CET) in directional solidification of dendritic alloys were determined in alloy systems such as Pb–Sn [10], Al–Cu [11], Al–Si [12], Al–Mg [13,14], Al–Zn and Zn – Al alloys [15]. These experiments allowed us to determine that the transition does not occur in an abrupt form in the samples and that it is present when the gradient in the liquid ahead of the columnar dendrites reaches critical and minimum values, being negative in most of the cases. In addition, we observed that two interphases, assumed to be macroscopically flat, are defined: the liquidus and the solidus interphases. After CET, the speed of the liquidus front accelerates much faster than the speed of the solidus front. Also, the average supercooling values were measured in these previous works [14]. A semi-empirical model was developed to predict the CET based on experimental results obtained from measurements made during solidification of lead–tin alloys directly upwards [16].

In addition, we have previously correlated the thermal parameters, type of structure, grain size and dendritic spacing with corrosion resistance of Zn–4 wt%Al, Zn–16 wt%Al and Zn–27 wt%Al alloys [17].

With respect to the correlation of structures with their mechanical properties, Osório et al. [6] analyses the mechanical properties of Zn–1 wt%Al, Zn–3 wt%Al and Zn–4 wt% Al alloys as a function of microstructure.

They determined experimental equations for these alloys relating ultimate tensile strength and yield strength with secondary dendrite arm spacing.

In a previous work on Zn – Al alloys (Zn–1 wt%Al, Zn–4 wt%Al, Zn–16 wt%Al, Zn–27 wt%Al) we found a linear and direct correlation between the mechanical properties YS, MTS and VH and secondary dendrite arm spacing, independent of the type of grains (columnar or equiaxed). YS, MTS and VH depend on the grain size and on the region considered: columnar or equiaxed [18].

* Corresponding author at: University of Misiones, 1552 Félix de Azara Street, 3300 Posadas-Misiones, Argentina. Fax: +54 3752 425414.
E-mail addresses: aares@fceqyn.unam.edu.ar, a.e.ares@gmail.com (A.E. Ares).

0022-0248/$ - see front matter © 2010 Elsevier B.V. All rights reserved.
doi:10.1016/j.jcrysgro.2010.11.112

The main objective of this paper is to confirm the influence of solidification conditions on the structure of pure Zn and Al, and Zn–Al (ZA) alloys in a wide range of concentrations, in particular the structures of the columnar, equiaxed and CET regions and the mechanical resistance (MTS, YS and UTS) of the different alloys and structures. The relations of the tensile parameters with the thermal parameters during solidification and the type of structure obtained are presented and discussed.

2. Experimental

2.1. Directional solidification and determination of structure and thermal parameters

The casting assembly used in the solidification experiments has been described previously [10–15]. The Zn and Al samples and Zn–3 wt%Al (ZA3), Zn–10 wt%Al (ZA10), Zn–15 wt%Al (ZA15), Zn–30 wt%Al (ZA30), Zn–37 wt%Al (ZA37) and Zn–50 wt%Al (ZA50) alloy samples were solidified directionally upwards. To ensure reproducibility of the results, three samples (140–150 mm high and 22.5 mm in diameter) were directionally solidified for each composition. The temperature was measured using K-type thermocouples protected with Pyrex® glass. The distance between the thermocouples was set at 20 mm.

After solidification, the samples (Fig. 1 (a)) were cut in the longitudinal direction, polished with emery paper to reveal the grain structure, etched using concentrated hydrochloric acid for 30 s at room temperature, followed by rinsing and wiping off the resulting black deposit. To reveal the microstructures, the samples were etched with a mix containing chromic acid (50 g Cr_2O_3 and 4 g Na_2SO_4 in 100 mL of water) for 10 s at room temperature [19].

The position of the CET was located by visual observation and optical microscopy, and the distance from the bottom of the sample was measured with a ruler. A typical resulting macrograph can be seen in Fig. 1(b) for Zn–3 wt%Al alloy. The microstructure was analyzed using SEM and an image processing system (Neophot-32 and Leica Q500 MC Cambridge) was then used to determine the average dendritic arm spacings performing 15 measurements in each selected position. The spacings were measured by counting the number of branches (primary (λ_1) or secondary (λ_2)) along a line of known length.

The equiaxed grain size (Gs) was measured using the ASTM E112 standard norm [20] at equally spaced intervals. The columnar region was divided in similar way and the width and length of the grains measured directly. The secondary arm spacing was measured in cross sections of the other half of the sample. Each section was mounted, polished and etched and the spacing was determined by the number of interceptions in a straight line.

The temperature profiles were determined from the measurements during solidification at different thermocouple positions. As reported before [10–15], these profiles allow the calculation of cooling velocity in the melt as the average value of the slopes. The start and the end of solidification at each thermocouple determine the positions of the liquidus and solidus solidification fronts versus

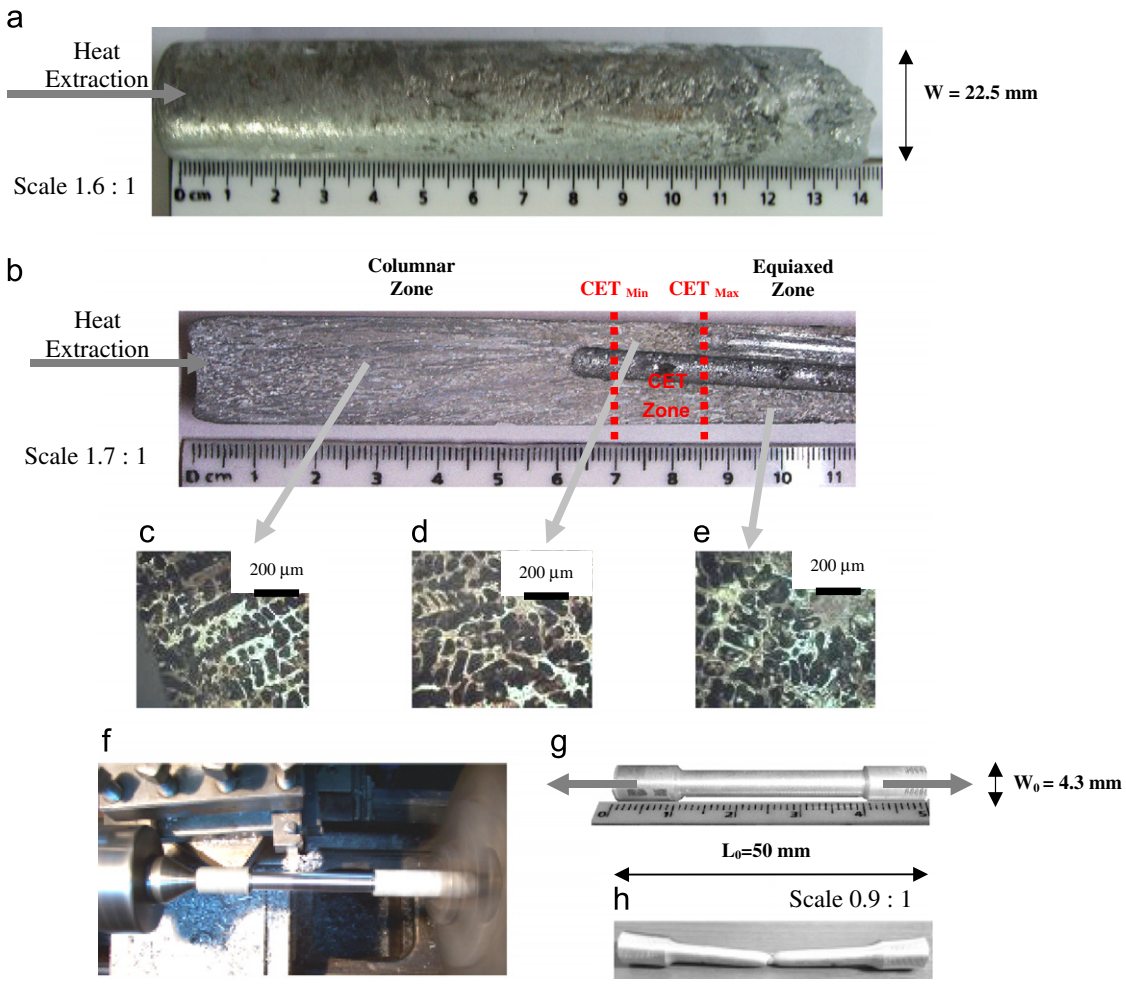

Fig. 1. (a) Sample of Zn–3 wt%Al alloy. (b) Macrostructure showing the columnar-to-equiaxed transition (CET). (c)–(e) Representative microstructures of each section, showing columnar and equiaxed dendrite zones and the dendrites in the CET zone. (f)–(h) Details of sample preparation according to ASTM /E-8M Norm.

time, which correspond to the liquidus and solidus temperatures, respectively. Both points are detected by the changes in the slopes of the cooling curve at the start and end of solidification.

The liquid and solid thermal gradients at all times are calculated straightforward, dividing the temperature difference between two thermocouples by the separation distance between them.

2.2. Tensile tests

The specimens were cut from directionally solidified samples and machined to the shape and size indicated in Fig. 1(f)–(h), i.e. a length (L_0) of 50 mm and an initial diameter (w_0) of 4.3 mm, following the standards given by ASTM /E-8 M [21] norms and using a SHIMADZU tensile test machine with a strain rate of 0.1 s^{-1}. The tensile direction was parallel to the growth direction. To ensure reproducibility of results, six specimens were tested for each alloy composition and structure.

After the test, each sample was cut, polished and etched [20] and the macro- and microstructure in the fracture zone were observed and analyzed (grain size and secondary dendrite arm spacing). The same procedure was followed for each sample.

3. Results and discussion

3.1. Solidification structure and CET determination and parameters

As reported previously the transition is not sharp, showing a zone where some equiaxed grains coexist with columnar grains [10–15]. In the present experiments, the size of the transition zone is up to 10 mm between the start of the CET (CET_{min} and the end of the CET (CET_{max}). Typical results of the transition are shown in Fig. 1 (b)–(e) for Zn–3 wt%Al. In Fig. 1(a) the ingot after solidification is shown and in Fig. 1(b) the macrostructure of the same ZA alloy sample is shown. Also, Fig. 1(c)–(e) shows microstructures of each section, showing columnar (c) and equiaxed (e) dendrite zones and the dendrites in the CET zone (d).

The thermal parameters extracted from the present experiments (i.e., cooling rate ($\dot{T}$), liquidus interphase velocity (V_L) and temperature gradient (G)) are presented in Table 1. As reported previously [10–13], when CET occurs in the sample, some of these parameters, such as the critical interphase velocity (V_{LC},) and the critical temperature gradient (G_C), become minimum and critical.

The CET in Zn–Al alloys presents aspects similar to those of other alloys. Some of these aspects are (a) the transition occurs in a zone delimited by a CET_{min} and a CET_{max} (rather than in a sharp plane), where both columnar and equiaxed grains coexist in the melt; the values in Table 1 correspond to the average of CET_{min} and CET_{max} ($CET_{average}$), which, in accordance to that previously reported [3,10–15,24], increases when the aluminum concentration increases; (b) the length of the columnar zone increases with the cooling rate and alloy composition and (c) the temperature gradient and the velocity of the liquidus front reach low critical values before the transition.

3.2. Measurement of structural parameters

The grain size was determined from a typical histogram showing the frequency of the size of the columnar and equiaxed grains; for each and all the size intervals the grain size was determined [10–15].

It is observed that the spacing steadily increases with distance from the bottom of the sample and rapidly increases at the top, where there is a transition from columnar to equiaxed; however, in the equiaxed zone it increases or remains approximately constant.

The increase in λ_1 from the chill zone of the sample is due to the corresponding decrease in the cooling rate ($\dot{T}$). It is observed that λ_1 increases steadily in the columnar and CET regions, then it either increases steadily in the equiaxed region or becomes constant. If we analyze the effect of the aluminum concentration, λ_1 decreases

Table 1

Zinc–aluminum alloy, type of structure obtained, average values of position of the CET ($CET_{average}$), thermal parameters: cooling rate ($\dot{T}_{average}$), liquidus interphase velocity ($V_{Laverage}$) and temperature gradient ($G_{Laverage}$) and parameters obtained from the tensile tests for each experiment with different type of structures (maximum tensile strength (MTS), yield strength (YS) and ultimate tensile strength (UTS)).

#	Alloy	Type of structure	$CET_{average}$ (mm)	$\dot{T}_{average}$ (K/s)	$V_{Laverage}$ (mm/s)	$G_{Laverage}$ (K/mm)	MTS (MPa)	YS (MPa)	UTS (MPa)
1	100 wt%Zn	Columnar	–	2.47	0.74	6.47	296.14	59.21	197.19
2	100 wt%Zn	Equiaxed	–	1.53	1.65	1.37	256.73	51.68	211.28
3	Zn–3 wt%Al	Columnar	–	2.65	0.83	9.15	238.7	86.15	129.17
4	Zn–3 wt%Al	CET	52.5	1.73	1.54	−0.27	181.23	60.26	86.84
5	Zn–3 wt%Al	Equiaxed	–	1.69	1.93	1.93	182.16	54.92	109.37
6	Zn–10 wt%Al	Columnar	–	2.45	0.99	5.87	204.69	76.16	116.12
7	Zn–10 wt%Al	CET	69.2	1.82	1.26	−1.43	172.41	50.2	85.27
8	Zn–10 wt%Al	Equiaxed	–	1.61	2.23	2.26	176.26	44.2	96.54
9	Zn–15 wt%Al	Columnar	–	2.12	0.66	8.31	169.06	60.05	91.00
10	Zn–15 wt%Al	CET	70.3	1.95	1.8	−1.05	145	45.12	84.61
11	Zn–15 wt%Al	Equiaxed	–	1.57	2.54	1.72	117.53	34.12	78.14
12	Zn–30 wt%Al	Columnar	–	2.63	0.92	3.84	165.62	48.09	93.27
13	Zn–30 wt%Al	CET	72.4	2.22	2.18	−0.56	163.54	43.24	72.28
14	Zn–30 wt%Al	Equiaxed	–	1.71	2.91	1.89	138.43	38.26	66.19
15	Zn–37 wt%Al	Columnar	–	2.98	1.01	4.82	116.14	55.11	103.78
16	Zn–37 wt%Al	CET	77.9	2.59	1.78	−0.02	112.67	52.73	82.56
17	Zn–37 wt%Al	Equiaxed	–	1.47	2.69	1.17	128.73	41.88	67.83
18	Zn–50 wt%Al	Columnar	–	2.85	1.17	5.53	156.24	46.25	90.49
19	Zn–50 wt%Al	CET	73.1	2.78	1.96	−0.18	139.51	42.83	62.21
20	Zn–50 wt%Al	Equiaxed	–	1.73	2.57	2.39	128.37	31.28	67.10
21	100 wt%Al	Columnar	–	1.97	0.86	7.26	105.83	78.12	84.28
22	100 wt%Al	Equiaxed	–	1.17	1.25	2.64	88.92	41.68	60.27

with the increase in Al concentration in agreement with previous research [11]. The relation becomes less clear in the transition zone. This behavior could be attributed to local effects since the solidification direction is random.

In addition, the secondary arm spacing (λ_2) was measured as a function of distance from the bottom of the sample. The increase in λ_2 is strictly related to the increase in local solidification time for all concentrations [6,11].

As shown by the temperature readings, in the present experiments the solidification time increases from the start of solidification towards the end at the top, as the macrostructure changes from columnar to equiaxed. The increase in solidification time is produced by a larger acceleration of the liquidus interphase with respect to the solidus interphase [10–15]. This acceleration is associated with the fast nucleation of the equiaxed grains after the start of the CET. On the other hand, increase in the aluminum content of the ZA alloy naturally increases the difference between the liquidus (T_L) and solidus (T_S) temperatures, which, in turn, increases the local solidification time for similar cooling rates.

3.3. Relation between thermal and structural parameters

The correlation between the average grain size in both zones (width of columnar grains for columnar zone and diameter of equiaxed grains for equiaxed zone) and the cooling rate was realized using the following equations: $G_s = a\dot{T}^{-b}$ (a and b are fitting parameters) and $\dot{T} = dT/dt$, which is the cooling rate during solidification, reported as K/mm.

The values of the constant for the columnar structure are higher than the values of the constant for the equiaxed structure. For both types of structures, the values of constant a decrease as the aluminum concentration increases. The constant b decreases from 5.52 for pure Zn to 1.2 for ZA50 alloy and 1.42 for pure Al for columnar structure and from 1.96 to 1.12 for equiaxed structure. Similar correlations were obtained for the primary and secondary dendrite arm spacings. The fact that the correlating function is non-linear indicates that very low cooling rates yield very wide grains and dendrite structures.

As reported before [10–15], experimental exponential growth laws were obtained correlating the mean values of λ_2 as a function of local solidification time (t_{SL}). The predictions by Feurer ($\lambda_2 = ct_{SL}^{1/3}$) [22] and Grugel ($\lambda_2 = 10t_{SL}^{1/2}$) [23] were included in the analysis for comparison purposes. The model of Feurer gives a better fit with our experiments, while the Grugel model predicts the values higher than the spacings measured. The constant c from the correlation of λ_2 with t_{SL} using the Feurer model, which uses the inverse cube root relationship, decreases from 10.51 for Zn–3 wt%Al to 8.65 for Zn–50 wt%Al.

3.4. Relation between mechanical parameters and thermal and structural parameters

From a typical tensile test, the values of maximum tensile strength (MTS), yield strength (YS) and ultimate tensile strength (UTS) were obtained. The values of MTS, YS, UTS and the type of structure in the fracture zone (columnar, CET and equiaxed) are listed in Table 1.

After the tensile test, the macro- and microstructure in the fracture zone were observed and analyzed (grain size and secondary dendrite arm spacing). The microstructures of the fracture zone of different samples are presented in Fig. 2. The fracture is fragile

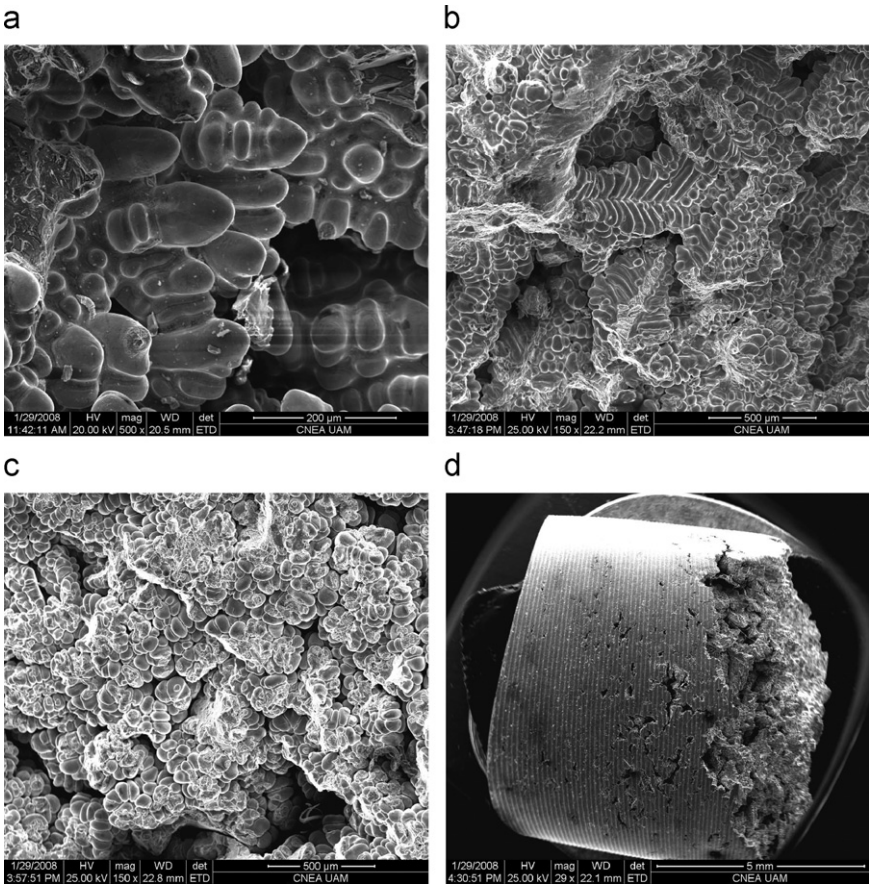

Fig. 2. Microstructures of the fracture zone of different samples: (a) columnar sample of Zn–3 wt%Al, (b) CET sample of Zn–15 wt%Al alloy, (c) equiaxed sample of Zn–10 wt%Al alloy and (d) Zn–50 wt%Al alloy sample showing porosity in the fracture zone.

and intragranular in the columnar zone (Fig. 2(a)) and always near some defect or porosity. The fracture is interdendritic in both types of structures (columnar and equiaxed; see Fig. 2 (b)). In the equiaxed zone, the fracture is granular in most cases (Fig. 2(c)). The porosity and superficial defects increase with the aluminum content in the alloy and in the equiaxed zone of the samples (this leads to a decrease in the TS), as it is possible to appreciate for Zn–50 wt%Al alloy in Fig. 2(d).

Table 1 and Fig. 3 show that MTS, YS and UTS decrease as the aluminum concentration increases.

The values of the correlation between YS and grain size are shown in Fig. 4(a). For a given grain size, the strengths are higher for the columnar zone. When analyzing the values for each type of structure separately, we observed that YS decreases as grain size increases; however, the relation differs in the region considered (columnar or equiaxed).

The values of the constant d from the linear correlation $Y_s = dG_s = e$ decrease from 36.82 (Zn–3 wt%Al) to 6.19 (Zn–50 wt%Al) and the values of e vary from 15.12 (Zn–3 wt%Al) to 1.52 (Zn–50 wt%Al) for the columnar zone. The values of the constants for the equiaxed zone vary between 19.63 (Zn–3 wt%Al) to 1.53 (Zn–50 wt%Al) and 14.33 (Zn–3 wt%Al) to 0.57 (Zn–50 wt%Al).

This correlation is not in concordance with the Hall–Petch relation [7,8], which predicts that as the grain size decreases the yield strength increases, according to $y_s = Y_{s0} + k(\text{grain size})^{-0.5}$. The relation was experimentally found to be an effective model for materials with equiaxed grain sizes ranging from 1 mm to 1 μm. In our experiments, the grain sizes measured are between 0.40 and 3.69 mm.

The values obtained by plotting YS as a function of λ_2 are shown in Fig. 4(b) for one alloy. In this case, it was possible to find a linear relation between YS and λ_2 as for columnar and equiaxed structures ($Y_s = f\lambda_2 + g$); these lines was determined for all alloy concentrations and structures. The parameter f decreases from 4.28 (Zn–3 wt%Al) to 1.52 (Zn–50 wt%Al) and g from 31.56 (Zn–3 wt%Al) to 5.58 (Zn–50 wt%Al) for columnar structure. In the case of the equiaxed structure the constants decrease from 4.01 (Zn–3 wt%Al) to 1.03 (Zn–50 wt%Al) and from 18.23 (Zn–3 wt%Al) to 1.13 (Zn–50 wt%Al). No relationships were found in the case of TS versus grain size and λ_2.

In order to correlate mechanical parameters with thermal parameters, three tensile strength (TS) parameters (MTS, YS and UTS) were plotted against cooling rate (Fig. 5(a)). This figure shows that the cooling rate increases, so does TS. The three parameters presented higher values for the columnar structure. The values of the CET structures are between columnar and equiaxed grain structures.

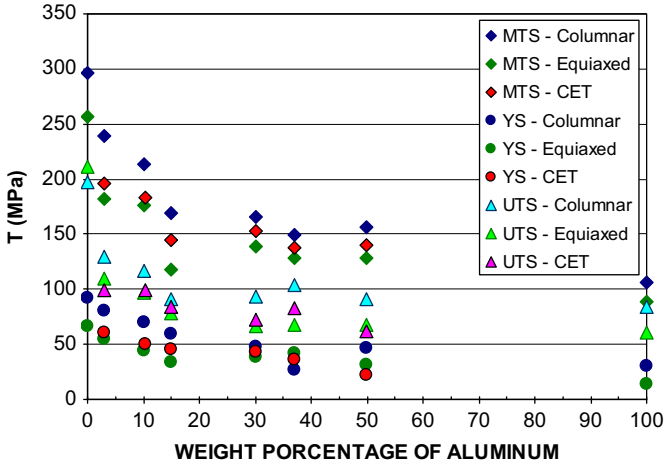

Fig. 3. Maximum tensile strength (MTS), yield strength (YS) and ultimate tensile strength (UTS) versus weigth percentage of aluminum.

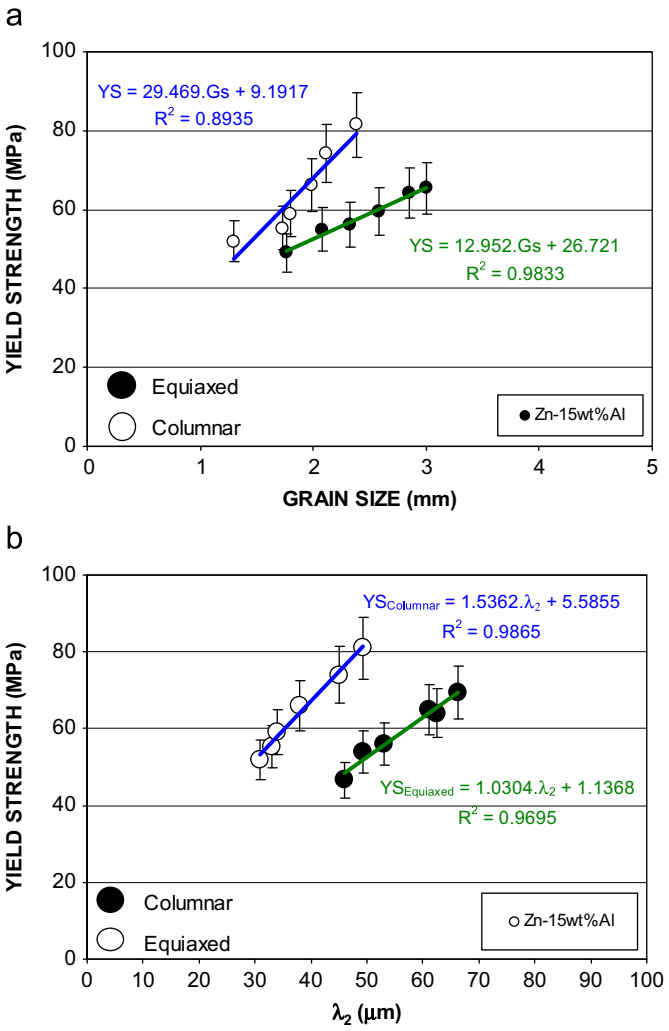

Fig. 4. Yield strength (YS) versus (a) grain size and (b) secondary dendritic arm spacing; Zn–15 wt%Al alloy.

The correlations between MTS, YS and UTS and cooling rate ($\dot{T}$) for all alloys was obtained as $TS = h\dot{T}^i$. It is observed for MTS and YS that the values of constant h decrease as the alloy concentration increases, and that the values of the constant i increase as Al concentrations increase. No correlation was found when correlating UTS with $\dot{T}$.

Fig. 5(b) shows TS against temperature gradient. The higher values of TS and temperature gradients were found for the columnar zone. The values of TS for the CET and equiaxed zones are lower. The correlation between MTS, YS and UTS and GL for all alloys as $TS = jG_L^k$, with values of the constant j decreasing with the alloy concentration only in the case of MTS versus G_L.

Fig. 6 shows the average values of different parameters (thermal, tensile and structural) as a function of position in the sample for Zn–15 wt%Al alloy. In order to obtain the correlations of different parameters (tensile, thermal and structural) in this figure, the stresses at various positions of the ingots were obtained by cutting six small samples of 50 mm height and 4.3 mm diameter (Fig. 1(g)) for tensile tests from three cylindrical ingots of 140–150 mm height and 22.5 mm diameter directionally solidified (Fig. 1(a)).

Consequently, the stress values were determined at different positions with respect to the bottom of the sample (metal/chill interface). In the figure it is possible to see that in the columnar zone the values of tensile parameters (MTS and YS) are high and also the values of cooling rate and temperature gradient but in the

case of the liquidus interphase velocity the values are lower. In this condition the macro- (columnar grain size) and microstructure (λ_1 and λ_2) are finer. In the equiaxed zone of the sample MTS and YS are lower than in the columnar zone, which is coincident with low values of cooling rate and temperature gradient but with higher liquidus interphase velocity. The equiaxed structure increases the size from the CET zone to the top of the sample.

Finally, when the CET occur, all parameters take intermediate values between those of the columnar and equiaxed zone except the value of temperature gradient in the liquid, which becomes minimum, critical and negative (the vertical axis of the Fig. 6 is in logarithm scale and the value of the temperature gradient at the CET is not present in the figure); the structure consists of large columnar grains, which stop growing for the nucleation and growth of small equiaxed grains.

This behavior in the analyzed parameters is comparable to that of the other directionally solidified alloys, with structures changing from columnar (base of the sample) to columnar-to-equiaxed transition (approximately in the middle of the sample) and finally equiaxed structure (at the top of the sample).

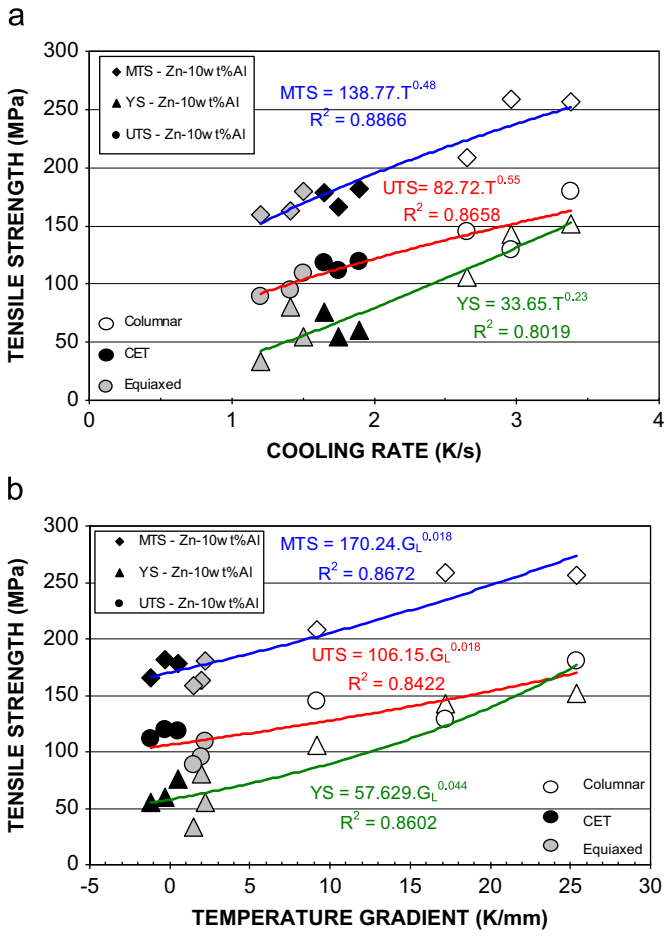

Fig. 5. Tensile strengths versus (a) cooling rate and (b) temperature gradient; Zn–10 wt%Al alloy.

4. Conclusions

From the results and discussion of the previous sections the main conclusions of this investigation on the correlation between different thermal and structural parameters and tensile parameters in Zn–Al alloys are

1. CET in Zn–Al (Zn–3 wt%Al, Zn–10 wt%Al, Zn–15 wt%Al, Zn–30 wt%Al, Zn–37 wt%Al and Zn–50 wt%Al) alloys presents aspects similar to those of the other previously studied alloys.
2. Mechanical properties MTS and YS depend on thermal and structural parameters, and on the region considered (columnar or equiaxed). Linear expressions correlating YS with structural parameters (grain size and secondary dendritic arm spacing) were obtained. Also, expressions as $TS = h\dot{T}^{i}$ and $TS = jG_L^k$ correlating MTS, YS and UTS with thermal parameters (cooling rate and temperature gradient) were obtained.
3. This study shows that the solidified structure obtained is strongly dependent on the thermal conditions during the solidification process and that the values of the tensile parameters depend on the kind of structure.

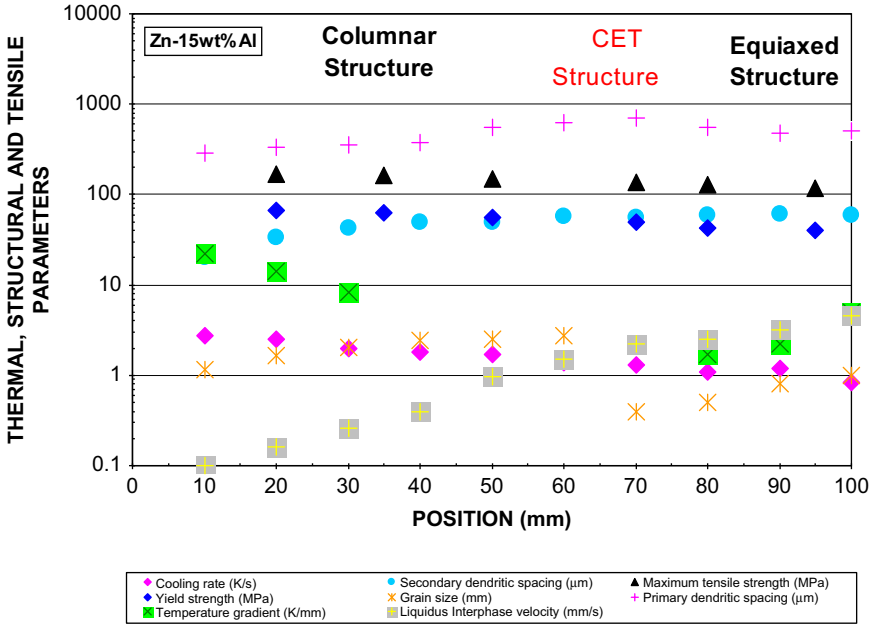

Fig. 6. Variation in average values of thermal and structural parameters with tensile parameters along the position in the sample; Zn–15 wt%Al alloy.

Acknowledgement

We thank the Argentinean Research Council (CONICET) for the financial support.

References

[1] L.A.J. Lodder, in: A.J. Murphy (Ed.), Non-Ferrous Foundry Metallurgy, Mc Graw Hill, New York,1954, p. 445.
[2] J.C. Fox, Zinc: The Science and Technology. Its Alloys and Compounds, Reinhold Publishing, New York, 1959, pp. 321–324.
[3] J.E. Spittle, International Materials Reviews 51 (2006) 247–269.
[4] ASTME 8M, Standard Test Methods for Tension Testing of Metallic Materials, American Society of Testing and Materials, 1995.
[5] J.T. Berry, AFS Transactions 78 (1970) 421–428.
[6] W.R. Osório, C.A. Santos, J.M.V. Quaresma, A. Garcia, Journal of Materials Processing Technology 143–144 (2003) 703–709.
[7] E.O. Hall, Proceedings of the Physical Society 71 B (1951) 747–752.
[8] N.J. Petch, Journal of the Iron and Steel Institute 174 (1953) 25–31.
[9] W.R. Osório, A. Garcia, Materials Science and Engineering 325A (2002) 103–111.
[10] A.E. Ares, C.E. Schvezov, Metallurgical and Materials Transactions 31A (2000) 1611–1625.
[11] A.E. Ares, S.F. Gueijman, C.E. Schvezov, Journal of Crystal Growth 312 (2010) 2154–2170.
[12] A.E. Ares, C.T. Rios, R. Caram, C.E. Schvezov, Dendrite spacing in Al–Cu and Al–Si–Cu alloys as function of the growth parameters, in: Wolfgang Schneider (Ed.), Light Metals, The Minerals, Metals and Materials Society, 222 Rosewood Drive, Danvers, MA 01923 USA, , 2002, pp. 785–792.
[13] A.E. Ares, R. Caram, C.E. Schvezov, Columnar-to-equiaxed transition studies in aluminum–magnesium and aluminum–zinc alloys, in: P. Crepeau (Ed.), Light Metals, The Minerals, Metals and Materials Society, 222 Rosewood Drive, Danvers, MA 01923, USA, , 2003in: P. Crepeau (Ed.), Light Metals, The Minerals, Metals and Materials Society, 222 Rosewood Drive, Danvers, MA 01923, USA, 2003, pp. 1047–1054.
[14] A.E. Ares, S.F. Gueijman, R. Caram, C.E. Schvezov, Journal of Crystal Growth 275 (2005) 235–240.
[15] A.E. Ares, C.E. Schvezov, Metallurgical and Materials Transactions 38A (2007) 1485–1499.
[16] A.E. Ares, S.F. Gueijman, C.E. Schvezov, Journal of Crystal Growth 241 (2002) 235–240.
[17] A.E. Ares, L.M. Gassa, S.F. Gueijman, C.E. Schvezov, Journal of Crystal Growth 310 (2008) 1355–1361.
[18] A.E. Ares, I.P. Gatti, S.F. Gueijman, C.E. Schvezov, Mechanical properties of zinc–aluminum alloys versus structural and thermal parameters, in: S.L. Cockcroft, D.M. Maijer (Eds.), Modelling of Casting, Welding and Advanced Solidification Processes – XII, The Minerals, Metals and Materials Society, 222 Rosewood Drive, Danvers, MA 01923, USA, , 2009, pp. 659–666.
[19] G.F. Vander Voort, Metallography Principles and Practice, ASM International, New York, 2000, pp. 528–761.
[20] H.E. Boyer, T.L. Gall, Metals Handbook, Desk Edition, American Society for Metals, 1990, 35-18–35-19.
[21] Tensile Test ASTM /E-8M Norm. Standard Test Methods for Tension Testing of Metallic Materials, American Society of Testing and Materials, 1995.
[22] U. Feurer, The Symposium on Quality Control of Engineering Alloys, Delft, vol. 131, 1977.
[23] R.N. Grugel, Journal of Materials Science 28 (1993) 677.
[24] Ch.A. Gandin, Acta Materialia 48 (2000) 2483–2501.